The Astrophysical Journal, 908:219 (9pp), 2021 February 20 https://doi.org/10.3847/1538-4357/abd554

Can Galaxy Evolution Mimic Cosmic Reionization?

Sultan Hassan[1,2,3,5] and Max Gronke[4,6]
[1] Center for Computational Astrophysics, Flatiron Institute, 162 5th Ave, New York, NY 10010, USA; shassan@flatironinstitute.org
[2] Department of Astronomy, New Mexico State University, Las Cruces, NM 88003, USA
[3] Department of Physics & Astronomy, University of the Western Cape, Cape Town 7535, South Africa
[4] Department of Physics & Astronomy, Johns Hopkins University, Baltimore, MD 21218, USA
Received 2020 September 30; revised 2020 December 11; accepted 2020 December 18; published 2021 February 25

Abstract

Lyα emitting galaxies are powerful tools to probe the late stages of cosmic reionization. The observed sudden drop in Lyα fraction at $z > 6$ is often interpreted as a sign of reionization, since the intergalactic medium (IGM) is more neutral and opaque to Lyα photons. Crucially, this interpretation of the observations is only valid under the assumption that galaxies themselves experience a minimal evolution at these epochs. By modeling Lyα radiative transfer effects in and around galaxies, we examine whether a change in the galactic properties can reproduce the observed drop in the Lyα fraction. We find that an increase in the galactic neutral hydrogen content or a reduction in the outflow velocity toward higher redshift both lead to a lower Lyα escape fraction, and can thus mimic an increasing neutral fraction of the IGM. We furthermore find that this change in galactic properties leads to systematically different Lyα spectra which can be used to differentiate the two competing effects. Using the CANDELSz7 survey measurements which indicate slightly broader lines at $z \sim 6$, we find that the scenario of a mere increase in the galactic column density toward higher z is highly unlikely. We also show that a decrease in outflow velocity is not ruled out by existing data but leads to more prominent blue peaks at $z > 6$. Our results caution using Lyα observations to estimate the IGM neutral fraction without accounting for the potential change in the galactic properties, e.g., by mapping out the evolution of Lyα spectral characteristics.

Unified Astronomy Thesaurus concepts: Reionization (1383); Galaxy evolution (594); Lyman-alpha galaxies (978); Intergalactic medium (813); Radiative transfer (1335)

1. Introduction

Lyα line is a promising tool to probe cosmic reionization as the increasingly neutral intergalactic medium (IGM) becomes more opaque to Lyα photons toward higher redshifts (e.g., for extensive reviews see Dijkstra 2014; Dayal 2019; Ouchi et al. 2020). This increased optical depth is expected to give rise to a decrease in the observed number of Lyα emitting galaxies at $z \gtrsim 6$. Specifically, the number of Lyα selected galaxies (or Lyα emitters, LAEs) decreases dramatically at this redshift (e.g., Ota et al. 2010; Tilvi et al. 2010; Matthee et al. 2014; Santos et al. 2016; Konno et al. 2018). Similarly, continuum selected, or Lyman break galaxies (LBGs) show a modest increase of Lyα emission from $z \sim 3$ to $z \sim 6$ (e.g., Hayes et al. 2011; Sobral et al. 2018), and sudden drop at $z \geqslant 6$ (Stark et al. 2011; Treu et al. 2013; Caruana et al. 2014; Pentericci et al. 2014, 2018; Schenker et al. 2014; Tilvi et al. 2014; De Barros et al. 2017; Mason et al. 2018, 2019; Hoag et al. 2019; Jung et al. 2020; Kusakabe et al. 2020). In particular, the latter is a powerful observational probe—as the Lyman break techniques allows the efficient detection of high-z galaxies—and is commonly parametrized by the "Lyα fraction" which describes the fraction of LBGs possessing a Lyα equivalent width $W > W_c$ where W_c is an observationally determined cutoff, usually 20 Å.

These different Lyα based observations are being used to constrain the evolution of the cosmic neutral fraction (Furlanetto et al. 2006; McQuinn et al. 2007; Dayal et al. 2011; Kakiichi et al. 2016; Mason et al. 2018, 2019; Naidu et al. 2020; Whitler et al. 2020; Morales et al. 2021). In fact, at $z \sim 7$ these measurements pin the neutral fraction to, for instance, $\langle x_{\rm H\,I} \rangle \approx 0.59^{+0.11}_{-0.15}$ (1σ error; taken from Mason et al. 2018; other studies such as the ones mentioned above use a different set of assumptions and, thus, conclude a different evolution of $x_{\rm H\,I}$) and are, thus, currently more constraining than measures of the cosmic microwave background (Planck Collaboration et al. 2016) or quasar proximity zones (e.g., Greig et al. 2017; Davies et al. 2018; Wang et al. 2020; Yang et al. 2020).

However, these constraints are crucially dependent on the assumption that the average *galactic* Lyα escape fraction does not change over this redshift interval as the observed Lyα flux is proportional to this times the intergalactic transmission. Therefore, an evolution in the cosmic neutral fraction is fully degenerate with the evolution of the Lyα escape fraction. While on the one hand, the duration from $z = 7$ to $z = 6$ is merely ~170 million years, i.e., relatively short in terms of galaxy evolution, one should keep in mind that this notion stems from studies carried out at lower redshifts.

Importantly, Lyα is a resonant line with a large cross section which implies that Lyα escape through the interstellar and circumgalactic medium is a highly nonlinear process. Several theoretical studies have shown that Lyα escape is dependent not only on the dust and neutral hydrogen abundance (Neufeld 1990; Dijkstra et al. 2006) but also on its kinematics (Bonilha et al. 1979; Zheng & Wallace 2014), and structure (Neufeld 1991; Gronke et al. 2017), and that even small changes in these properties can have large effects on the Lyα observables—and, in particular, the escape fraction.

Independently of the question whether the currently employed assumption of a constant Lyα escape fraction with redshift is justified, it is important to incorporate our ignorance

[5] Flatiron fellow.
[6] Hubble fellow.

regarding the evolution of the interstellar and circumgalactic medium into the models constraining cosmic evolution (see work by Papovich et al. 2011, Finkelstein et al. 2012, suggesting a larger accretion rate leading to a larger gas reservoir, and thus, lower Lyα escape fraction). Sadoun et al. (2017) took a first stride at this goal by demonstrating that the observed drop in Lyα fraction can be entirely due to the increased neutral hydrogen content in the infalling region surrounding the dark matter halo hosting the galaxy. While in their interpretation this increased neutral fraction is due to a change in the ionizing background—and, thus, arguably also a sign of cosmic reionization—this result is very important as it shows the potential impact of this change of Lyα transmission not stemming from an evolution of the IGM.

In this paper, we want to systematically explore what changes in galactic properties can mimic the observed evolution of Lyα visibility usually attributed to the Epoch of Reionization. We will, furthermore, study how such changes will impact the Lyα spectra. This will allow future studies to use these additional constraints, and thus allow them to fold in the uncertainty regarding the galactic evolution into the models.

This paper is organized as follows: in Section 2, we describe the quantities and the radiative transfer code used, in Section 3 we present our results, and we discuss them in Section 4.

2. Methods

2.1. Lyα Fraction

As stated above, the Lyα fraction, $X_{\mathrm{Ly}\alpha}$, is commonly defined as the fractional abundance of galaxies with Lyα equivalent width (W) above certain cut-off (W_{c}), which can be written as:

$$X_{\mathrm{Ly}\alpha,\mathrm{W}_c} = \int_{W_c}^{\infty} p(W)\, dW, \tag{1}$$

where $p(W)$ is the equivalent width distribution function. As commonly used in the literature (Dijkstra & Wyithe 2012; Gronke et al. 2015; Sadoun et al. 2017), we adopt an exponential form for $p(W)$:

$$p(W) = \frac{\exp(-W/W_0)}{W_0 + W_1} \qquad \text{for } W > 0, \tag{2}$$

where W_0 and W_1 are free parameters, which can be found by matching to observations. It has been found that this parameterization reproduces observations reasonably well (Schenker et al. 2014).[7]

By integrating Equation (1) using two different observationally motivated thresholds $W_{\mathrm{c}} = 25$, 55 Å, the exponential scale W_0 becomes:

$$W_0 = \frac{30\ \text{Å}}{\ln(X_{\mathrm{Ly}\alpha,25}/X_{\mathrm{Ly}\alpha,55})}. \tag{3}$$

The W_0 is M_{UV} magnitude dependent as observations indicate. Using the measured Lyα fractions at $z = 6$ by Stark et al. (2011), we find $W_{0,z=6} = 43.3$, 30.2 Å for the faint ($M_{\mathrm{UV}} > -20.25$) and bright ($M_{\mathrm{UV}} < -20.25$) populations, respectively. We will use this $W_{0,z=6}$ value for the faint population throughout. By doing so, we match the observed Lyα fraction measurement at $z = 6$. We then attempt to reproduce the observed drop in Lyα fraction at $z > 6$ by changing only the galactic properties.

In general, the observed Lyα equivalent width W is given by

$$W = \frac{f_{\mathrm{esc,Ly}\alpha}}{f_{\mathrm{esc,\ UV}}} T_{\mathrm{IGM}}\, W_{\mathrm{i}}, \tag{4}$$

where T_{IGM} is the IGM transmission, W_{i} is the intrinsic equivalent width, and $f_{\mathrm{esc,Ly}\alpha}$ and $f_{\mathrm{esc,\ UV}}$ are the photon escape fractions for Lyα and UV photons, respectively. We assume that the IGM does not evolve (i.e., $T_{\mathrm{IGM}} = $ const., see Section 4 for more details), and the dust optical depth τ_{d} is the same at $z \geqslant 6$, which also keeps the $f_{\mathrm{esc,\ UV}}$ constant ($f_{\mathrm{esc,\ UV}} = \exp(-\tau_{\mathrm{d}})$). With these assumptions, we can translate the change in the equivalent width distribution to change in the Lyα photon escape fraction. By simultaneously solving the Lyα fraction equations for $z = 6$ and $z > 6$, we obtain

$$\frac{f_{\mathrm{esc,Ly}\alpha}(z>6)}{f_{\mathrm{esc,Ly}\alpha}(z=6)} = \left[1 - \frac{W_{0,z=6}}{W_c} \log\left(\frac{X_{\mathrm{Ly}\alpha,c}(z>6)}{X_{\mathrm{Ly}\alpha,c}(z=6)}\right)\right]^{-1}. \tag{5}$$

This equation relates the change in the photon escape fraction to the change in the Lyα fraction between two redshifts. This relation depends on the equivalent width cut-off W_{c} and the exponential scale W_0 for the equivalent width distribution, which is magnitude dependent.

Here we focus on the measurements for the faint populations ($M_{\mathrm{UV}} > -20.25$) with cutoff $W_c > 25$ Å. Our results might be quantitatively different for the bright population, but nevertheless the qualitative result will remain unchanged, which is that the main focus for the work is to test the scenarios with which the change in the galactic properties can mimic reionization sign. We will come to this point later, in the discussion.

There are several measurements for the Lyα fraction at $z \geqslant 6$. For simplicity, we take the average values from Stark et al. (2011) and De Barros et al. (2017) at $z \sim 6$, Pentericci et al. (2014), Schenker et al. (2014), Caruana et al. (2014), Mason et al. (2018) at $z \sim 7$, Tilvi et al. (2014), Treu et al. (2013), Schenker et al. (2014) and Mason et al. (2019) at $z \sim 8$. These average values of the Lyα fraction are 0.46, 0.24 0.14 at $z \sim 6$, 7, 8, respectively. Using Equation (5), these average values indicate that the photon escape fraction may equivalently drop by $f_{\mathrm{esc,Ly}\alpha}(z=7)/f_{\mathrm{esc,Ly}\alpha}(z=6) = 0.47$, and $f_{\mathrm{esc,Ly}\alpha}(z=8)/f_{\mathrm{esc,Ly}\alpha}(z=6) = 0.33$, to mimic the observed drop in Lyα fraction from $z = 6$ to $z = 7$ and $z = 6$ to $z = 8$, respectively. It is worth noting that if we use Pentericci et al. (2018) measurements at $z = 6$, which are lower than those compiled by Stark et al. (2011), to find the exponential scale W_0, the required drop would be $f_{\mathrm{esc,Ly}\alpha}(z=7)/f_{\mathrm{esc,Ly}\alpha}(z=6) = 0.53$, and $f_{\mathrm{esc,Ly}\alpha}(z=8)/f_{\mathrm{esc,Ly}\alpha}(z=6) = 0.39$. These values are still consistent within 1σ level of each other, and would not significantly alter our conclusion. Our aim is to study the conditions with which a change in the galactic properties leads to these differences in the photon escape fraction, and hence mimicking reionization. While uncertainties in the measurements do exist (see, e.g., Jung et al. 2020; Kusakabe et al.

[7] Note while we focus on the evolution in the Lyα fraction, a change in the observed equivalent widths, e.g., due to a change in galactic properties, $W \to aW$ leads to a change in the scale height $W_0 \to aW_0$. This means that our results can be understood as a change in the equivalent width distribution. The details depend naturally on the parameterization of the EW distribution.

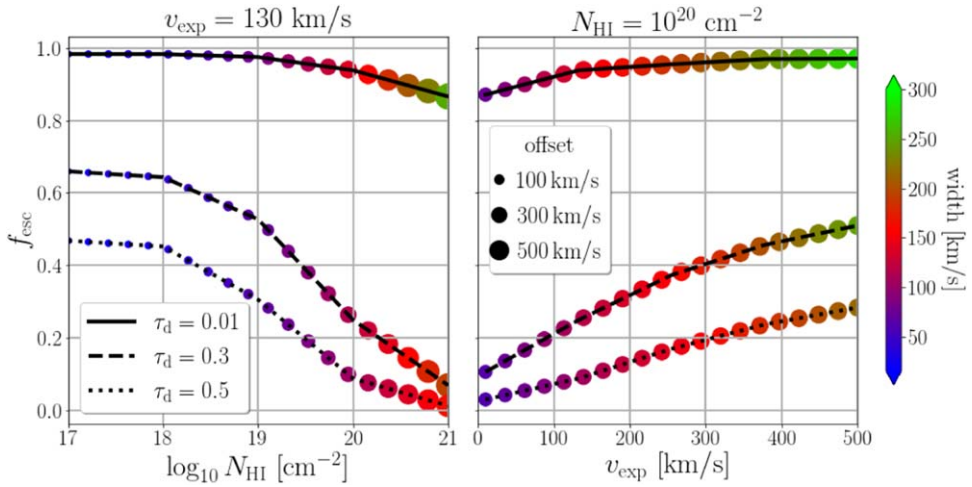

Figure 1. The Lyα photon escape fraction $f_{\rm esc}$ dependence on the galactic properties. *Left*: $f_{\rm esc}$ as a function of column density $N_{\rm H\,I}$ at fixed outflow velocity $v_{\rm exp} = 130$ km s^{-1}. *Right*: same as left but as a function of $v_{\rm exp}$ at a fixed $N_{\rm H\,I} = 10^{20}$ cm^{-2}. Different linestyles correspond to different dust amounts $\tau_{\rm d}$ as shown in the legend. Different colors and point sizes represent the spectral width (square root of second moment) of the red peak and offset of the red side of Lyα emission, respectively. $f_{\rm esc}$ decreases in denser and dustier media and increases with higher outflows. The width and offset both increase with increasing column density and outflow velocity. An increase in the column density $N_{\rm H\,I}$ or decrease in outflows $v_{\rm exp}$ toward high redshift ($z > 6$) by a factor of $\sim \times$ 2–3 reproduces the observed drop in Lyα fraction $X_{\rm Ly\alpha}$ and mimics the increase in neutral fraction (i.e., reionization) without an evolving IGM.

2020), the outcome of our theoretical study does not depend on the exact observationally inferred drop of the Lyα visibility. Instead, we want to explore here whether in principle such a drop can be reproduced by evolution of galactic properties.

2.2. Monte Carlo Lyα Radiative Transfer

We model Lyα emission from and around galaxies assuming shell models as implemented within a Monte Carlo radiative transfer (MCRT) code TLAC (Gronke & Dijkstra 2014). The MCRT methods tracks the evolution and properties of injected photons including direction and frequency as they travel through the simulation domain. The "shell-model" is commonly adopted as it has been shown to reproduce observed Lyα spectra well (Ahn et al. 2003; Verhamme et al. 2006; Gronke 2017).[8] It is defined by the neutral hydrogen column density $N_{\rm H\,I}$, the dust optical depth $\tau_{\rm d}$, the expanding/outflowing velocity $v_{\rm exp}$, and the effective temperature T. In all our runs, we consider an initial number of photon packages of $N = 10^5$ which we inject at line center, unless otherwise stated. We here consider two scenarios to the change in the galactic properties that can lead to a change in the photon escape fraction required to mimic reionization. While keeping all other properties fixed, these scenarios are changing only either the column density $N_{\rm H\,I}$ or the outflows $v_{\rm exp}$. We leave $T = 10^4$ K fixed for all the runs.

To this end, we have shown how the drop in Lyα fraction is equivalent to a drop in the photon escape fraction while keeping the IGM fixed. In the next section, we present our results relating the change in the galactic properties to the photon escape fraction and spectral properties, as well as comparing with observations to discriminate between these two scenarios.

[8] There is an ongoing discussion in the literature regarding the physical meaning behind the "shell-model" (e.g., Gronke et al. 2017; Orlitová et al. 2018). We will comment on the interpretation of our results in light of the adopted model in Section 4.

3. Results

3.1. Impact of Galactic Properties on f_{esc} and Lyα Spectra

Figure 1 is a visual summary of how the Lyα photon escape fraction $f_{\rm esc}$ and spectral properties change as the galactic properties evolve. We show the dust impact on $f_{\rm esc}$ with variation in the optical depth $\tau_{\rm d}$ as quoted in the legend and represented by different linestyles. We color-code $f_{\rm esc}$ dependence on the galactic properties ($N_{\rm H\,I}$ and $v_{\rm exp}$) with the width (square root of second moment), and the point sizes reflect the offset (the first moment) of the red side of Lyα emission.

The left panel of Figure 1 shows the $f_{\rm esc}$ dependence on the column density $N_{\rm H\,I}$ at a fixed outflow velocity $v_{\rm exp} = 130\,{\rm km\,s^{-1}}$, whereas the right panel depicts the dependence on the outflow velocity $v_{\rm exp}$ at a fixed column density $N_{\rm H\,I} = 10^{20}{\rm cm^{-2}}$. In general, $f_{\rm esc}$ decreases as the $N_{\rm H\,I}$ increases and $v_{\rm exp}$ decreases. Both a higher H I column density and a lower outflow velocity imply that the optical depth at line center increases, and thus, so does the path length of Lyα photons through the scattering medium. This in turn means that the effective dust optical depth increases, lowering the escape fraction.

Note that the $f_{\rm esc}$ dependence on $N_{\rm H\,I}$ is steeper than that on $v_{\rm exp}$. At small dust amounts (solid lines), $f_{\rm esc}$ is almost unity as most photons easily escape. In this regime, the galactic properties are required to change dramatically in order to observe a factor of 2 difference in $f_{\rm esc}$. With a dustier medium (dashed and dotted lines), it is easier to find such a difference with smaller change in the galactic properties. For instance, at $\tau_{\rm d} \geqslant 0.3$, a change by $\leqslant 1$ order of magnitude in $N_{\rm H\,I}$ or by $\leqslant 200\,{\rm km\,s^{-1}}$ in $v_{\rm exp}$ is needed to reduce $f_{\rm esc}$ by factor 2. We also see that the spectral properties such as the width and offset change accordingly. These changes can potentially be tested against observations (see Section 3.4 below). The width and offset both increase as the $N_{\rm H\,I}$ or/and $v_{\rm exp}$ increase. Similarly, the dependence on $N_{\rm H\,I}$ is steeper since we see the width changes from about $\sim 50\,{\rm km\,s^{-1}}$ at $\log_{10} N_{\rm H\,I}/{\rm cm^{-2}} = 17$ up to more than $500\,{\rm km\,s^{-1}}$ by $\log_{10} N_{\rm H\,I}/{\rm cm^{-2}} = 21$. Overall we find a tight correlation between offset and width, with the offset

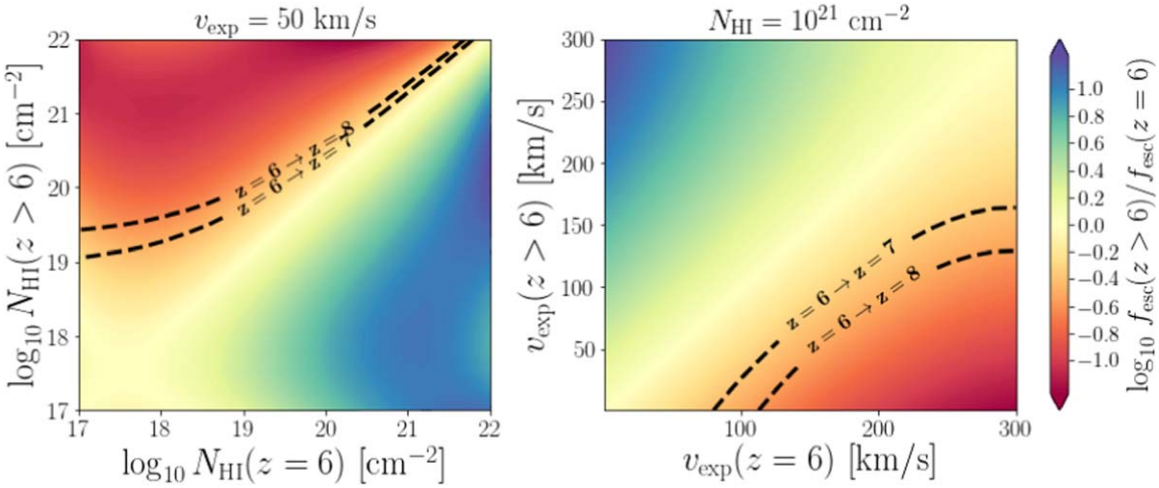

Figure 2. Grid of models with different column densities $N_{\rm H\,I}$ and fixed outflow velocity $v_{\rm exp} = 50$ km s^{-1} (left) and with different outflows $v_{\rm exp}$ at fixed column density $N_{\rm H\,I} = 10^{21}$ cm^{-2} (right), both at the same amount of dust $\tau_{\rm d} = 0.35$ at $z \geqslant 6$. The horizontal axis represents the column density and outflows at $z = 6$, whereas the vertical axis shows the same quantities at higher redshifts, $z = 7$, 8. Both panels are color-coded with photon escape fraction $f_{\rm esc}$ ratio between $z > 6$ and $z = 6$. Contours show the possible column densities/outflows between $z = 6 \rightarrow z = 7$ and $z = 6 \rightarrow z = 8$ with $f_{\rm esc}$ difference that mimics the sign of reionization as often inferred from the observed drop in Lyα fraction $X_{\rm Ly\alpha}$ at these epochs.

being roughly about ∼2 times the width, in agreement with previous studies (e.g., Neufeld 1990; Verhamme et al. 2018). Unsurprisingly, the spectral properties are mostly unaffected by the dust content. On the other hand, the line width dependence on $v_{\rm exp}$ is somewhat modest as it changes from 300 km s^{-1} at very low $v_{\rm exp} \sim 5$ km s^{-1} to about less than 500 km s^{-1} by $v_{\rm exp} \sim 500$ km s^{-1}. Likewise, the offset dependence on $N_{\rm H\,I}$ is more significant since point sizes change significantly toward high $N_{\rm H\,I}$ values as opposed to the slow change as the $v_{\rm exp}$ increases.

In summary, Figure 1 illustrates nicely the facts that (i) it is possible to find examples where the change in the galactic properties can reduce $f_{\rm esc}$ significantly, and (ii) that such a change is accompanied by a change in Lyα spectral properties. The questions now are if these changes in $f_{\rm esc}$ are sufficient to reproduce the observed sudden drop in Lyα fraction $X_{\rm Ly\alpha}$ without an evolving IGM, and if—or rather—in which parameter range these changes in galactic properties are realistic.

3.2. Escape Fraction Variation Consistent with the Change in $X_{Ly\alpha}$

As can already be seen from the previous section and Figure 1, the measured drop in $X_{\rm Ly\alpha}$ of ∼50% (∼70%) for $z \sim 6 \rightarrow 7$ ($z \sim 6 \rightarrow 8$) can be reproduced entirely by a change in galactic properties. To explore systematically for which parameters this is the case, we ran a grid of models and show explicitly in Figure 2 the change in escape fraction that is produced by a change in column density $N_{\rm H\,I}$ and outflow velocity $v_{\rm exp}$. We furthermore draw black contour lines representing the change needed to reproduce the observed $X_{\rm Ly\alpha}$ drop for a fixed choice of dust ($\tau_{\rm d} = 0.35$).

In the left panel of Figure 2, we vary the column density at a fixed outflow velocity of 50 km s^{-1}. Starting at low column density e.g., $N_{\rm H\,I} = 10^{17-18}$ cm^{-2} at $z = 6$, a rather large increase by ∼1–2 order of magnitudes is required to obtain the required ∼halving of $f_{\rm esc}$ by $z = 7$. On the other hand, for larger column densities $\log_{10} N_{\rm H\,I}/{\rm cm}^{-2} > 19$ a significantly smaller increase of < 1 dex in neutral hydrogen column density is necessary, sometimes $\lesssim$0.1 dex.

Similarly, in the right panel of Figure 2 we show what change in $f_{\rm esc}$ a change in outflow velocity produces while fixing $N_{\rm H\,I} = 10^{21}$ cm^{-2}. We see here contours representing the observed drop in $X_{\rm Ly\alpha}$ are located in the lower right part, which is opposite to the left panel. This shows that in order to mimic reionization with only the outflow velocity, higher outflows are required at low redshift ($z = 6$). The required change in outflows is about $\leqslant$100 km s^{-1} between these redshifts, which is somewhat moderate. While these models have fixed dust, outflow (left) and column density (right), we can easily predict the corresponding change in these contours for different choice of parameters. For instance, $f_{\rm esc}$ increases at lower dust values, which means that the contours in the left and right panels would be shifted accordingly to upper and lower part of the grid. Higher outflows increase $f_{\rm esc}$ and hence the contours would shift to the lower part in the left panel, whereas higher column density would shift the contours in the right panel to the upper part.

In this section, we showed that both a change in column density and a change in outflow velocity can reproduce the observed drop in Lyα detections at $z \gtrsim 6$ usually attributed to an increased neutral hydrogen content of the IGM at these epochs. We furthermore explored how the change in the galactic properties can mimic an increasing neutral fraction with a change in $f_{\rm esc}$. A change consistent with the measured drop of the Lyα fraction toward $z > 6$ can be achieved either by boosting the column density by ∼0.1 dex for $N_{\rm H\,I} \gtrsim 10^{19}$ or suppressing outflows toward high redshift. We next discriminate between these scenarios using the change in the spectral properties.

3.3. Lyα Spectral Line Properties Variation as a Function of the Galactic Properties

As already visible from Figure 1, the change in the galactic properties that mimics reionization does not only produce a different $f_{\rm esc}$, but also changes significantly the Lyα spectral line properties which can be tested against observations.

Figure 3 shows several examples for the variation in Lyα spectral line properties between redshift $z = 6$ and $z = 7$ at the same amount of dust, $\tau_{\rm d} = 0.2$. Top row shows the resulting

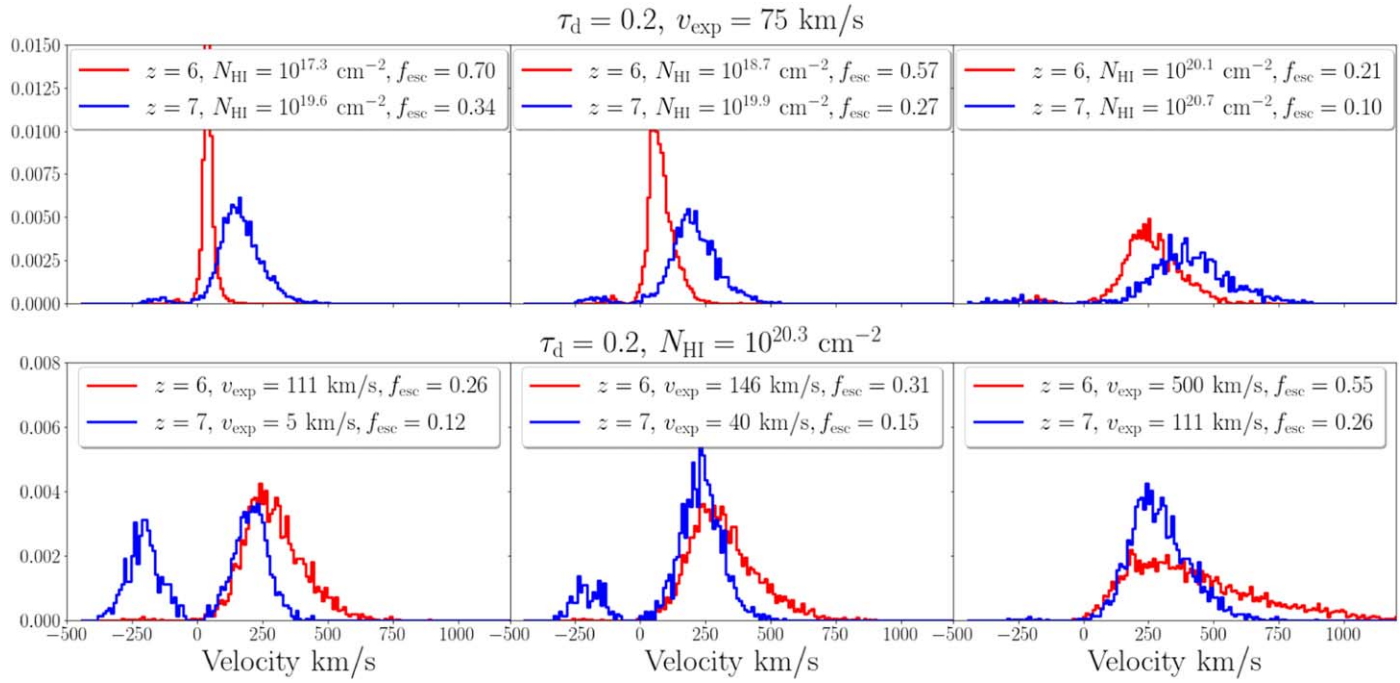

Figure 3. Several examples for the change in spectral properties between $z = 6$ (red) and $z = 7$ (blue) as the galactic properties change at a fixed amount of dust $\tau_d = 0.2$ with a pixel resolution of 10 km s^{-1}. Top row shows the change in column density $N_{H\,I}$ at fixed outflows v_{exp}, whereas the bottom row shows the opposite as quoted in the legend and subtitles. In all panels, the difference in f_{esc} is equivalent to the observed drop in Lyα fraction $X_{Ly\alpha}$ between $z = 6$ and $z = 7$. In the top row, the line width and offset both increase as the column density increases toward high-z, whereas the bottom row indicates that the line width and offset both decrease as the velocity decreases toward high-z. Note that we focus on the most extreme scenario in which the visibility on Lyα at $z > 6$ is purely due to galaxy evolution. Thus, an unobscured IGM transmission was assumed (see Section 4 for a discussion of this effect).

spectral changes due to changing the column density $N_{H\,I}$ at fixed outflows v_{exp}, whereas the bottom row depicts the opposite scenario. All these examples possess the required $\sim\times 1/2 f_{esc}$ difference between $z = 6$ and $z = 7$ to mimic the drop in the observed Lyα fraction $X_{Ly\alpha}$ as explained in the previous section.

In the top panels of Figure 3, we show that the scenario of changing the column density to mimic reionization suggests that the line width and offset both increase toward high redshift. It is also noted that the line is broader at higher column densities. Interestingly, the second scenario of changing the outflows shown in the lower row of Figure 3 indicates exactly the opposite, that broader lines exist at higher outflow velocities, i.e., at lower redshifts. This is due to the fact that increasing the column density also increases the escape frequency offset at which Lyα can escape through excursion (Neufeld 1990). On the other hand, for outflowing material a fraction of photons are "backscattered" and obtain $\sim$2 the expansion velocity (Dijkstra et al. 2006; Verhamme et al. 2006). This produces the extended red wings in Figure 3 and implies that a lower outflow velocity produces narrower line widths. It is also evident that the blue peak appears more prominently with decreasing outflows to small values, consistent with previous studies (Bonilha et al. 1979). This means that the two considered scenarios (changing $N_{H\,I}$ or v_{exp}) to mimic reionization can be distinguished with observations of Lyα spectra. We explore this in detail in the next section.

3.4. Comparison to Observations

We now use observations to discriminate between our two scenarios. Using the CANDELSz7 survey, Pentericci et al. (2018) have measured the line widths of two stacks of 52 sources with $\langle z\rangle \sim 6$ and 19 other sources with $\langle z\rangle \sim 7$, and found that their full width at half maximum (FWHM) are equal to 300 ± 30 km s^{-1} and 220 ± 25 km s^{-1}, respectively. This shows that these observations indicate that line width is approximately constant or slightly decreasing with increasing redshift. Recalling the results of the previous section, this automatically rules out the scenario of changing the column density $N_{H\,I}$ to mimic reionization since it predicts that the line width increases toward high redshift.

We now explore this more quantitatively as well as check whether a change in outflow velocity or the column density and an associated drop in escape fraction is consistent with the line width measurements of Pentericci et al. (2018).

To do so, we attempt to follow the recipe presented in Pentericci et al. (2018) to produce stacks of mock spectra using our model at $z = 6$ and $z = 7$. Using an initial number of photons of $N_{photon} = 10^4$, we run a grid of 1125 models over five different amounts of dust ($\tau_d = 0.1$–0.5), 15 outflows ($v_{exp} = 5$–500 km s^{-1}) and 15 column densities ($\log_{10} N_{H\,I} = 17$–21 cm^{-2}); all equidistantly spaced. By considering all possible combinations at fixed column density and dust content, we then select those whose difference in f_{esc} is equivalent to the observed drop in $X_{Ly\alpha}$ between $z = 6$ and $z = 7$. We find 650 or 1036 combinations of models at $z = 6$ and $z = 7$ satisfying these requirements in changing the outflows or column density scenarios, respectively. Out of these models, we ignore combinations that are inconsistent (i.e., with FWHM $> \pm 2\sigma$) with Pentericci et al. (2018) measurements at $z \sim 6$. This reduces the number of models combinations to 143 and 201 in the case of changing the outflows and column density, respectively. This means that the presented results here by construction are consistent with $z = 6$ observations, and we aim to explore the different scenarios

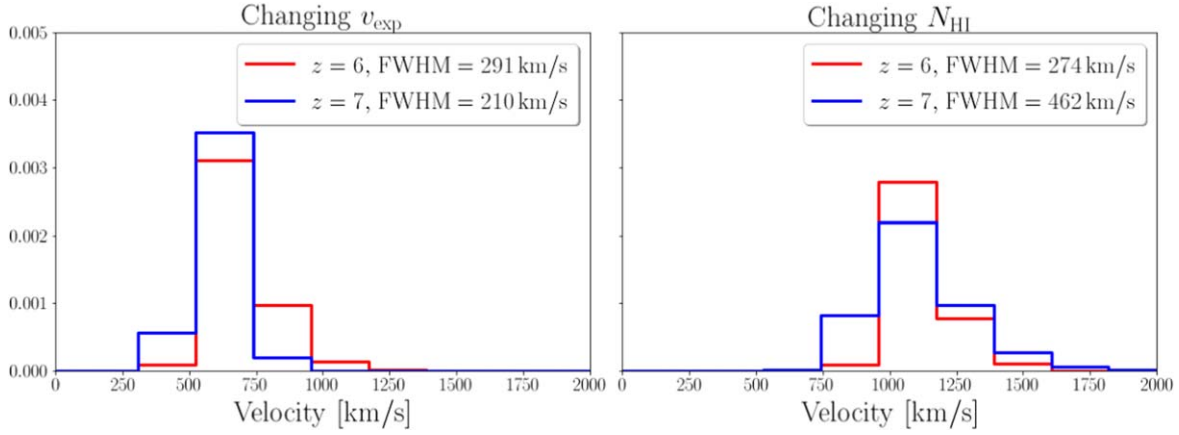

Figure 4. Example for stacks of randomly selected 52 mock spectra at $z = 6$ (red) and 19 mock spectra at $z = 7$ (blue) with $f_{\rm esc}(z = 7) \approx 0.5 f_{\rm esc}(z = 6)$ in agreement with the measured drop of $X_{\rm Ly\alpha}$. We assembled the stacks following the method outlined in Pentericci et al. (2018) with spectral resolution $R = 1390$ (corresponding to $\Delta = 216$ km s^{-1}). All these spectra are either obtained by changing only outflows $v_{\rm exp}$ while keeping the column density $N_{\rm H\,I}$ fixed (left) or changing only the column density $N_{\rm H\,I}$ while keeping outflows $v_{\rm exp}$ fixed. In all cases, dust is kept fixed. In either scenario, the FWHM of stacks at $z = 6$ is consistent with values reported in Pentericci et al. (2018, FWHM($z \sim 6$) = 300 ± 30). The FWHM of stacks obtained by changing outflows $v_{\rm exp}$ at $z = 7$ is also consistent with Pentericci et al. (2018) measurements (FWHM($z \sim 7$) = 220 ± 25) while those produced by changing the column density $N_{\rm H\,I}$ are not, and hence indicating that changing the outflow $v_{\rm exp}$ can naturally lead to a higher Lyα escape as well as broader lines at lower redshifts as observations indicate.

predictions at high-z as compared with measurements. Similar to Pentericci et al. (2018), we bin all spectra using a spectral resolution of $R = 1390$, corresponding to velocity resolution of $\Delta v = 216$ km s^{-1}, and produce median stacks of randomly selected 52 spectra at $z = 6$ and only 19 spectra at $z = 7$. We also add noise to each individual spectrum drawn from Gaussian distribution of zero mean and standard deviation set by the signal-to-noise ratio of S/N = 5 per pixel (i.e., $\sigma_i = F_i/5$ where F_i is the flux of pixel i). We show two random examples for stacks of this procedure at $z = 6$ (red) and $z = 7$ (blue) in Figure 4 as obtained by changing only the outflows (left) or changing only the column density (right). While both scenarios produce stacks that have consistent FWHM values with observations at $z = 6$, the changing outflows scenario yields also a consistent FWHM with $z = 7$ measurements. This also confirms that changing the column density predicts very high FWHM >400 km s^{-1} at $z = 7$. As quoted in the legend for changing the outflows scenario (left), $z = 6$ lines are broader than those at $z = 7$, and consistent with Pentericci et al. (2018). The lines are highly asymmetric with extended red wings. The blue peaks disappear due to the poor resolution.

To quantify the width using the above recipe, we generate randomly 10,000 combination of stacks at $z = 6$ and $z = 7$ from the total number of model combinations (i.e., 143 and 201) in each scenario and compute their widths. We show the resulting width distribution at these redshifts in Figure 5. Results from changing outflows and changing column density scenarios are presented by dashed and solid lines. Shaded red and blue areas show Pentericci et al. (2018) measurements at $z \sim 6$ and $z \sim 7$, respectively. From this exercise alone, we constrain the FWHM, using changing column density scenario, to 261.7 ± 14.3 km s^{-1} at $z = 6$ and 434.9 ± 47.8 km s^{-1} at $z = 7$, and using changing outflows scenario, to 291.5 ± 7.9 km s^{-1} $z = 6$ and 224.6 ± 22.8 km s^{-1} at $z = 7$. It is evident that, over all possible combinations and the prior range assumed, the changing outflows scenario produces consistent width distribution within the 1σ level of Pentericci et al. (2018) measurements. This confirms that changing the column density predicts inconsistent width distributions. It might be noteworthy that while we use the Pentericci et al. (2018) results in this section, other studies of the spectral properties at that redshift might obtain different results due to a different sample selection.

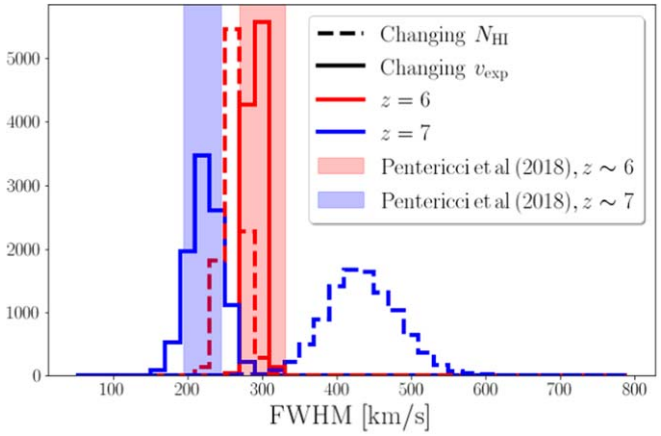

Figure 5. Line width distribution using randomly generated 10,000 stacks at $z = 6$ (red) and $z = 7$ (blue) obtained by changing only the outflows (solid) or changing only the column density (dashed). Shaded red and blue areas show Pentericci et al. (2018) measurements at $z \sim 6$ and $z \sim 7$, respectively. It is evident that the scenario of changing the outflows is consistent with the observations, while changing the column density scenario predicts very high FWHM values at $z \sim 7$.

We now use these scenarios to make predictions for the blue/red flux ratio, which is defined as the total blue line flux divided by the total red flux. We perform these predictions at the level of individual spectra not with stacks, since the blue peaks disappear due to the poor resolution. We show the blue/red flux ratio distribution from total number of model combinations in Figure 6. Both scenarios produce similar flux ratio at $z = 6$. However, changing the outflows scenario predicts higher flux ratio at $z = 7$, indicating the presence of more blue peaks at high redshift, which is opposite to the change in column density scenario. Note that for this paper we explore the somewhat extreme scenario where the entire change of the Lyα visibility is due to galaxy evolution alone, i.e., we assume a completely transparent IGM. In reality, the majority of the IGM at $z \gtrsim 5$ is already opaque to Lyα photons

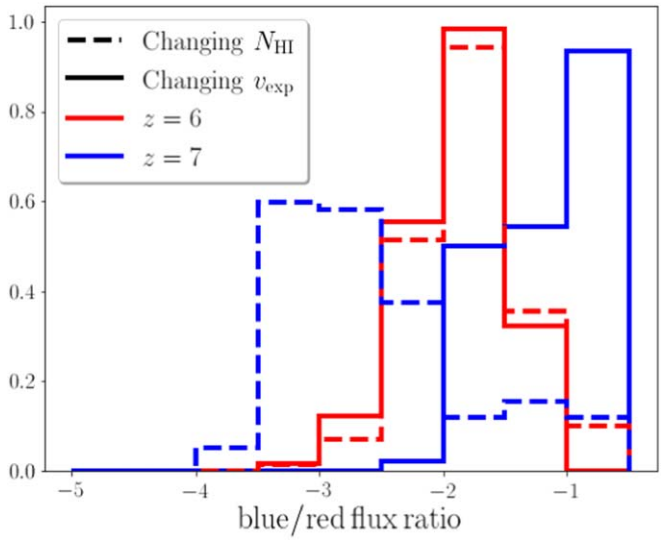

Figure 6. Predictions for the blue/red flux ratio at $z = 6$ (red) and $z = 7$ (blue) for changing the column density scenario (dashed) or changing the outflows (solid). Both scenarios produce similar flux ratio at $z = 6$. Changing the outflows scenario predicts higher flux ratio at $z = 7$, indicating the presence of more blue peaks at high redshift, which is opposite to the change in column density scenario.

blueward of line center. This means that an enhancement of the blue peak toward higher z can be translated to a lower observed Lyα visibility (even with non-evolving IGM) and, thus, to a reduction of the required change of galactic properties in order to reproduce the observed change in EW(Lyα). We will discuss this further in Section 4.

4. Concluding Remarks

The decrease in Lyα visibility for $z > 6$ is commonly interpreted as a change in IGM opacity due to the Epoch of Reionization. As an alternative, we have explored scenarios of how the change in the galactic properties can naturally lead to drop in the photon escape fraction that is equivalent to the observed drop in Lyα fraction while keeping the IGM fixed at $z \geqslant 6$. We have considered two scenarios: changing the column density $N_{\rm H\,I}$ or the outflow velocity $v_{\rm exp}$. We found that decreasing the column density by only $\lesssim$1 dex ($\lesssim$0.1 dex for $N_{\rm H\,I} \gtrsim 10^{19}\,{\rm cm}^{-2}$) or increasing the outflow velocity by $\sim$100 km s^{-1} with decreasing redshift can both successfully reproduce the observed drop in the Lyα fraction, and thus, "mimic" an increasing IGM neutral fraction. Note that these exact values depend on the observed drop in $X_{{\rm Ly}\alpha}$. We have adopted values consistent with most studies (see Section 2) but note that recent work by Kusakabe et al. (2020) have reported much lower value of Lyα fraction at $z \sim 6$ of $X_{{\rm Ly}\alpha} = 0.13$, which is less than Stark et al. (2011) by a factor of 4. Naturally this would lead to a smaller evolution in the explored galactic properties, but since the primary goal of this study is to show whether in principle an observed drop in Lyα visibility can be explained by galaxy evolution (independent of the exact redshift it occurs at) these yet existing observational differences do not alter our conclusion.

To differentiate between the evolution in galactic and intergalactic properties, we analyze the associated change in Lyα spectral properties. The line width and offset both increase as the column density and outflows increase. The observed spectral properties can potentially discriminate between these scenarios, which indicate that the broader lines exist in low redshift (Pentericci et al. 2018). This automatically rules out the changing column density scenario (see Section 3.4). On the other hand, the scenario of a change in outflow properties does not alter the spectral width significantly, and is thus compatible with current observations. Following Pentericci et al. (2018), we generate 10,000 stacks and compare to the observed width results. We find the line width is 291.5 ± 7.9 km s^{-1} at $z = 6$ and 224.6 ± 22.8 km s^{-1} at $z = 7$, which is consistent with the 1σ level of the Pentericci et al. (2018) measurements. We predict that such a scenario of a change in outflow properties implies a larger flux on the blue side of Lyα toward higher redshifts. While in principle this could be directly detectable—and there has been an increasing number of blue peaks at high-z has been detected (Hu et al. 2016; Matthee et al. 2018; Songaila et al. 2018; Bosman et al. 2020)—the IGM already at $z \lesssim 5$ is already mostly opaque to Lyα photons on the blue side altering systematically the observed spectra (Laursen et al. 2011; Byrohl & Gronke 2020; Hayes et al. 2021). Such an evolution would thus have to be indirect, i.e., through the (change in) Lyα halo properties.

Throughout this study, we model the complex radiative transfer through the galactic and circumgalactic medium by the simple concentric, outflowing shell. While this "shell-model" has been shown to reproduce observed Lyα spectra well,[9] there is an ongoing discussion in the literature why this is, and what the shell-model parameters represent (e.g., Gronke et al. 2017; Orlitová et al. 2018; Li et al. 2021). While a full discussion of the problem is beyond the scope of this work, we want to highlight some points most relevant for this study. In particular, both theoretical (Dijkstra et al. 2016; Eide et al. 2018; Kakiichi & Gronke 2019) as well as observational work (J.-B. Vielfaure et al. 2020, in preparation) points toward the fact that Lyα spectra are in a way an extremum statistics, i.e., they are heavily weighted toward low opacity channels. This is maybe unsurprising as Lyα photons most easily escape through these "pathways of least resistance." Specifically, from this theoretical work it became clear that Lyα spectra can be shaped by the lowest column densities channels—even when this is not along the line-of-sight toward the observer (e.g., Eide et al. 2018).[10] This implies for our study that not the average galactic properties but instead the "extreme" (in terms of opacity) has to evolve in order to mimic reionization. As such, lower density or higher velocity channels can occur on relatively short timescales ($\lesssim$tens of Myr), for instance, due to a burst of star formation (Norman & Ikeuchi 1989; Sparre et al. 2017; Faisst et al. 2019), the required change in the "shell-model" parameters—in particular the outflow velocity—from $z \sim 6$ to ~ 7, 8 (>200 Myr) is in fact not unlikely. We expect future studies targeting the connection of the "shell-model" to more realistic gas geometries to allow improved estimates on their variability. While we argue that the "shell-model" represents a good model for Lyα radiative transfer in order to reproduce observed spectra, this is clearly not the case for the surface brightness (SB) profile (e.g., Song et al. 2020). A realistic SB profile could lead to additional non-observed Lyα photons due

[9] Something that cannot be claimed when using more complex input geometry, e.g., from galactic simulations (see discussion in Gronke et al. 2018; Mitchell et al. 2021) which further justifies the usage of the "shell-model" in this study.

[10] While observational confirmation is difficult as it requires an independent tracer of the H I column density, for instance, GRB afterglow spectra offer an attractive opportunity (Vielfaure et al. 2020).

to the SB limit of observations, however, this effect is beyond the scope of this paper, i.e., here we assume a non-evolving SB profile.

A limitation of this study is the homogeneous treatment of the galaxy population. A more realistic approach is to develop a novel approach, such abundance matching, to link the equivalent width distribution to the galaxy mass or stellar mass function at these epochs, and then study what change is required in the whole galaxy population to mimic the whole equivalent width distribution. We leave exploring possibilities to undertake such an approach in future works.

Additionally, the dust has been also assumed fixed in our analysis. To first order expected evolution of dust optical depth for Lyα photons is to follow the metallicity, i.e., to decrease toward high redshift. This in turn would increases the $f_{\rm esc,Ly\alpha}$, and goes in the opposite direction to the observed drop in $X_{\rm Ly\alpha}$. In our both scenarios, it is still possible to combine the increase of dust toward high redshift with the increase of column density of decrease in outflows, but these changes in the galactic properties would be larger to offset the evolution in dust. Given the uncertainty in dust and metallicity at these high redshift epochs, and general uncertainty of how does interacts with Lyα photons,[11] we have compared models at the same level of dust optical depth.

In summary, we have shown that the change in Lyα visibility toward higher redshift can be attributed to a change in galactic properties and does not require a change in IGM properties. Specifically, we find that both a modest decrease in column density (in agreement with Sadoun et al. 2017) or an increase in outflow velocity in the galaxies' evolution can lead to an increase in Lyα escape fraction, and thus, to the observed drop in detected Lyα emission toward $z > 6$. We furthermore found that this degeneracy between IGM transmission and galactic Lyα radiative transfer can be broken using the emergent Lyα spectral properties. In particular, we found that the scenario of a change in column density leads to unnatural wide Lyα profiles and is ruled out by existing data—but that the change in outflow properties is not. We predict that in such a case there will be more blue flux emergent from galaxies toward redshifts which can be detectable either directly or through an evolution in Lyα halo properties.

Naturally, a fast evolution of the IGM neutral fraction at $z > 6$ is expected and observed using other, independent probes, we caution that the uncertainty of galactic Lyα radiative transfer should be taken into account when constraining this evolution using the observed Lyα equivalent width distribution or luminosity function.

The authors acknowledge helpful discussions with Charlotte Mason, Daniel Stark, Edmund Christian Herenz and Steven Finkelstein, and thank the referee for constructive comments. This research made use of matplotlib (Hunter 2007), SciPy (Virtanen et al. 2020), IPython (Pérez & Granger 2007), and NumPy (Harris et al. 2020). Part of this work was performed during a research visit to the Space Telescope Science Institute (STScI) where support was provided by the STScI Directors Discretionary Fund. Simulations and analysis were performed at NMSU's DISCOVERY supercomputers. This work also used the Extreme Science and Engineering Discovery Environment (XSEDE), which is supported by National Science Foundation grant No. ACI-1548562, and computational resources (Bridges) provided through the allocation AST190003P. M.G. was supported by NASA through the NASA Hubble Fellowship grant HST-HF2-51409 and acknowledges support from HST grants HST-GO-15643.017-A, HST-AR-15039.003-A, and XSEDE grant TG-AST180036.

[11] How susceptible Lyα photons are to dust depends heavily its distribution and is focus of a large body of literature (e.g., Neufeld 1991; Hansen & Oh 2006).

ORCID iDs

Sultan Hassan https://orcid.org/0000-0002-1050-7572
Max Gronke https://orcid.org/0000-0003-2491-060X

References

Ahn, S.-H., Lee, H.-W., & Lee, H. M. 2003, MNRAS, 340, 863
Bonilha, J. R. M., Ferch, R., Salpeter, E. E., Slater, G., & Noerdlinger, P. D. 1979, ApJ, 233, 649
Bosman, S. E. I., Kakiichi, K., Meyer, R. A., et al. 2020, ApJ, 896, 49
Byrohl, C., & Gronke, M. 2020, A&A, 642, L16
Caruana, J., Bunker, A. J., Wilkins, S. M., et al. 2014, MNRAS, 443, 2831
Davies, F. B., Hennawi, J. F., Bañados, E., et al. 2018, ApJ, 864, 142
Dayal, P. 2019, in IAU Symp. 352, Uncovering Early Galaxy Evolution in the ALMA and JWST Era, 43
Dayal, P., Maselli, A., & Ferrara, A. 2011, MNRAS, 410, 830
De Barros, S., Pentericci, L., Vanzella, E., et al. 2017, A&A, 608, A123
Dijkstra, M. 2014, PASA, 31, e040
Dijkstra, M., Gronke, M., & Sobral, D. 2016, ApJ, 823, 74
Dijkstra, M., Haiman, Z., & Spaans, M. 2006, ApJ, 649, 14
Dijkstra, M., & Wyithe, J. S. B. 2012, MNRAS, 419, 3181
Eide, M. B., Gronke, M., Dijkstra, M., & Hayes, M. 2018, ApJ, 856, 156
Faisst, A. L., Capak, P. L., Emami, N., Tacchella, S., & Larson, K. L. 2019, ApJ, 884, 133
Finkelstein, S. L., Papovich, C., Salmon, B., et al. 2012, ApJ, 756, 164
Furlanetto, S. R., Zaldarriaga, M., & Hernquist, L. 2006, MNRAS, 365, 1012
Greig, B., Mesinger, A., Haiman, Z., & Simcoe, R. A. 2017, MNRAS, 466, 4239
Gronke, M. 2017, A&A, 608, A139
Gronke, M., & Dijkstra, M. 2014, MNRAS, 444, 1095
Gronke, M., Dijkstra, M., McCourt, M., & Peng Oh, S. 2017, A&A, 607, A71
Gronke, M., Dijkstra, M., Trenti, M., & Wyithe, S. 2015, MNRAS, 449, 1284
Gronke, M., Girichidis, P., Naab, T., & Walch, S. 2018, ApJL, 862, L7
Hansen, M., & Oh, S. P. 2006, MNRAS, 367, 979
Harris, C. R., Millman, K. J., van der Walt, S. J., et al. 2020, Natur, 585, 357
Hayes, M., Schaerer, D., Östlin, G., et al. 2011, ApJ, 730, 8
Hayes, M. J., Runnholm, A., Gronke, M., & Scarlata, C. 2021, ApJ, 908, 36
Hoag, A., Bradač, M., Huang, K., et al. 2019, ApJ, 878, 12
Hu, E. M., Cowie, L. L., Songaila, A., et al. 2016, ApJL, 825, L7
Hunter, J. D. 2007, CSE, 9, 90
Jung, I., Finkelstein, S. L., Dickinson, M., et al. 2020, ApJ, 904, 144
Kakiichi, K., Dijkstra, M., Ciardi, B., & Graziani, L. 2016, MNRAS, 463, 4019
Kakiichi, K., & Gronke, M. 2019, arXiv:1905.02480
Konno, A., Ouchi, M., Shibuya, T., et al. 2018, PASJ, 70, S16
Kusakabe, H., Blaizot, J., Garel, T., et al. 2020, A&A, 638, A12
Laursen, P., Sommer-Larsen, J., & Razoumov, A. O. 2011, ApJ, 728, 52
Li, Z., Steidel, C. C., Gronke, M., & Chen, Y. 2021, MNRAS, 502, 2389
Mason, C. A., Fontana, A., Treu, T., et al. 2019, MNRAS, 485, 3947
Mason, C. A., Treu, T., Dijkstra, M., et al. 2018, ApJ, 856, 2
Matthee, J., Sobral, D., Gronke, M., et al. 2018, A&A, 619, A136
Matthee, J. J. A., Sobral, D., Swinbank, A. M., et al. 2014, MNRAS, 440, 2375
McQuinn, M., Hernquist, L., Zaldarriaga, M., & Dutta, S. 2007, MNRAS, 381, 75
Mitchell, P., Blaizot, J., Cadiou, C., & Dubois, Y. 2021, MNRAS, 501, 5757
Morales, A., Mason, C., & Bruton, S. 2021, arXiv:2101.01205
Naidu, R. P., Tacchella, S., Mason, C. A., et al. 2020, ApJ, 892, 109
Neufeld, D. A. 1990, ApJ, 350, 216
Neufeld, D. A. 1991, ApJL, 370, L85
Norman, C. A., & Ikeuchi, S. 1989, ApJ, 345, 372
Orlitová, I., Verhamme, A., Henry, A., et al. 2018, A&A, 616, A60
Ota, K., Iye, M., Kashikawa, N., et al. 2010, ApJ, 722, 803
Ouchi, M., Ono, Y., & Shibuya, T. 2020, ARA&A, 58, 617
Papovich, C., Finkelstein, S. L., Ferguson, H. C., Lotz, J. M., & Giavalisco, M. 2011, MNRAS, 412, 1123
Pentericci, L., Vanzella, E., Castellano, M., et al. 2018, A&A, 619, A147

Pentericci, L., Vanzella, E., Fontana, A., et al. 2014, ApJ, 793, 113
Pérez, F., & Granger, B. E. 2007, CSE, 9, 21
Planck Collaboration, Adam, R., Aghanim, N., et al. 2016, A&A, 596, A108
Sadoun, R., Zheng, Z., & Miralda-Escudé, J. 2017, ApJ, 839, 44
Santos, S., Sobral, D., & Matthee, J. 2016, MNRAS, 463, 1678
Schenker, M. A., Ellis, R. S., Konidaris, N. P., & Stark, D. P. 2014, ApJ, 795, 20
Sobral, D., Santos, S., Matthee, J., et al. 2018, MNRAS, 476, 4725
Song, H., Seon, K.-I., & Hwang, H. S. 2020, ApJ, 901, 41
Songaila, A., Hu, E. M., Barger, A. J., et al. 2018, ApJ, 859, 91
Sparre, M., Hayward, C. C., Feldmann, R., et al. 2017, MNRAS, 466, 88
Stark, D. P., Ellis, R. S., & Ouchi, M. 2011, ApJL, 728, L2
Tilvi, V., Papovich, C., Finkelstein, S. L., et al. 2014, ApJ, 794, 5
Tilvi, V., Rhoads, J. E., Hibon, P., et al. 2010, ApJ, 721, 1853
Treu, T., Schmidt, K. B., Trenti, M., Bradley, L. D., & Stiavelli, M. 2013, ApJL, 775, L29
Verhamme, A., Garel, T., Ventou, E., et al. 2018, MNRAS, 478, L60
Verhamme, A., Schaerer, D., & Maselli, A. 2006, A&A, 460, 397
Vielfaure, J. B., Vergani, S. D., Japelj, J., et al. 2020, A&A, 641, A30
Virtanen, P., Gommers, R., Oliphant, T. E., et al. 2020, Nat. Method., 17, 261
Wang, F., Davies, F. B., Yang, J., et al. 2020, ApJ, 896, 23
Whitler, L. R., Mason, C. A., Ren, K., et al. 2020, MNRAS, 495, 3602
Yang, J., Wang, F., Fan, X., et al. 2020, ApJL, 897, L14
Zheng, Z., & Wallace, J. 2014, ApJ, 794, 116